Adaptive Photonic Microwave Instantaneous Frequency Estimation Using Machine Learning

Qidi Liu, Benjamin Gily, and Mable P. Fok, Member, IEEE

Abstract— Instantaneous microwave frequency estimation enables numerous essential applications in the commercial, defense, and civilian marketplace. The advancement of applications is hindered by the bottleneck in electronic-based frequency measurement systems including narrow bandwidth, high errors rate, and low dynamic range. Photonics-based frequency estimation approaches not only increase the operation frequency range and provide rapid measurement response, but also benefit from immunity to electromagnetic interference and enhancement in system adaptability. Despite the unique advantages offered by photonics-based frequency estimation approaches, it is challenging to obtain linear mapping between the unknown frequency and the measured optical characteristics due to the nonlinear response in electro-optical devices, which consequently results in degradation in measurement precision and a complex calibration relationship. Therefore, it is critical to mitigate the challenge to achieve dynamic, adaptive, and highprecision estimation of microwave frequency. To this end, this paper presents the design and demonstration of a high-precision photonic based instantaneous frequency estimation system driven by machine learning. A three-layer deep neural network is used to tackle device nonlinearity and system noise, resulting in absolute error of < 50 MHz and root mean square error of 1.1 MHz.

Index Terms—Frequency estimation, Machine learning

I. INTRODUCTION

Westimation system is an essential tool for radar detection, electronic warfare, military threats identification, decisive intelligence acquisition, and deceptive counter-measures implementation [1]. However, emerging wideband and complex wireless environment brings critical challenges to realize frequency estimation using conventional electronic technologies, resulting in narrow bandwidth, high errors rate, and low dynamic range measurements. The unique characteristic of photonic, including wideband operation, high reconfigurability, and instantaneous response make photonics be a promising candidate to overcome hurdles faced by electronics approaches. Microwave photonic based frequency estimation have been demonstrated using frequency-to-time

Manuscript received XXXX XX, 2021; revised XXXX XX, 2021; accepted XXXX XX, 2021. Date of publication XXXX XX, 2021; date of current version XXXX XX, 2021. This work was supported in part by the National Science Foundation under Grant 1653525, 1917043. (Corresponding author: Mable P. Fok.)

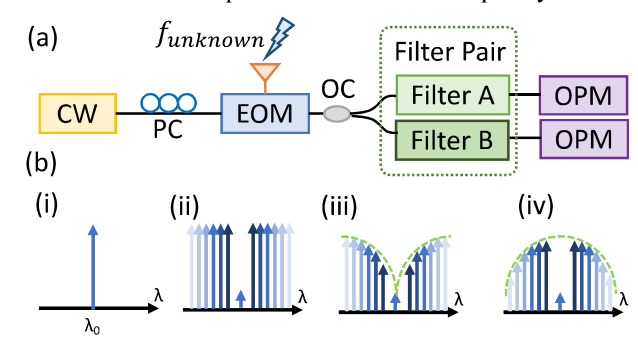
The authors are with the Lightwave and Microwave Photonics Laboratory, College of Engineering, The University of Georgia (UGA), USA (e-mail: qidi.liu@uga.edu; bwg58333@uga.edu; mfok@uga.edu). Color versions of one or more figures in this letter are available at https://doi.org/10.1109/LPT.2021.3067755.
Digital Object Identifier XX.XXXX/LPT.2021.XXXXXX

Fig. 1. Schematic of the basic photonic microwave frequency estimation system. CW: continuous wave; EOM: electro-optic modulator; PC: polarization controller. OC: optical coupler. (b) optical spectra of (i) optical

mapping [2], power fading comparison [3], SBS-assisted phase-to-intensity modulation [4], and frequency-to-intensity mapping [5]. Although existing photonic approaches solved some of the challenges that their electronic counterparts are facing, current photonic schemes suffer from relatively limited reconfigurability for optimizing measurement performance, large frequency estimation error in the order of hundreds of MHz, and inability to adapt to dynamic RF scenario.

At the same time, machine learning (ML) has been used to enhance a wide range of photonic signal processing tasks, including optical performance monitoring, nonlinearity compensation in transmission system, proactive fault detection, and software-defined networking [6]. Recently, a convolutional neural network-assisted optimization method is proposed to achieve instantaneous frequency estimation over the Brillouin frequency range (~10 GHz) and achieve significant accuracy improvement with error within several tens of MHz [7]. However, there is a trade-off between measurement range and tolerance error. Most existing frequency estimation methods could either enable wideband measurement range with relatively low frequency resolution (i.e. a few hundred MHz) or achieve a small error (i.e. tens of MHz) with narrow measurement range. In [8], we have obtained some preliminary results for demonstrating the feasibilty of machine learning in microwave photonic frequency estimation to improve measurement error performance. However, there is still a critical need to supply solid theoretical analysis, detailed simulation comparison as well as the practical implementation of the DNN-assisted frequency estimation model with dynamic parameters tuning (i.e. extinction ratio, free spectral range, varying electrical power).

In this letter, we principally and experimentally demonstrated an adaptive instantaneous frequency estimation



carrier, (ii) CS-DSB signal, (iii) (iv) filter pair (cosine shape).

system based on complementary optical power measurement assisted by deep neural network (DNN). Based on prior experience the intelligent frequency estimation system has, high measurement accuracy as well as high tolerance to device nonlinearity and system noise are achieved. The DNN-assisted frequency estimation system can adapt to dynamic RF transmission condition and significantly decrease the resultant frequency estimation error to 50 MHz with a 1.1-MHz root mean square error over a 14-GHz frequency range.

II. OPERATION PRINCIPLE

A. Basic Photonic Microwave Frequency Estimation

To perform microwave frequency estimation, the unknown microwave signal-of-interest is modulated onto an optical carrier via an electro-optic intensity modulator (EOM), as shown in Figure 1(a). The EOM is biased at the null transmission point to achieve carrier suppressed double sideband modulation (CS-DSB). The CS-DSB modulated optical output is then sent to an optical comb filter pair with complementary spectral responses (i.e. with positive and inverse responses). Therefore, the microwave frequency can be determined by monitoring the filtered optical powers using two optical power meters. Assuming the input electrical field amplitude is $E_0 exp(j2\pi f_c t)$, the CS-DSB optical signal resulted from an applied microwave signal at frequency f_{RF} can be written as,

$$\begin{split} E_{out}(t) &= E_0 \Sigma_n J_{2n}(\beta) \cos(2\pi f_c t + 2n \cdot 2\pi f_{RF} t \\ &- n\pi) + J_{2n-1}(\beta) \cos(2\pi f_c t \\ &- (2n-1) \cdot 2\pi f_{RF} t + n\pi) \end{split} \tag{1}$$

where $J_n(.)$ is the *n*-th Bessel function of the first order. It can be seen that amplitudes of the generated optical sidebands are proportional to the corresponding Bessel functions associated with the modulation depth $\beta = \pi \frac{V_m cos(2\pi f_{RF})}{v}$.

In conventional optical digital signal processing, the modulating microwave signal power and the nonlinear transfer function of modulator are ignored such that the assumption of the small signal modulation is satisfied, resulting in only the

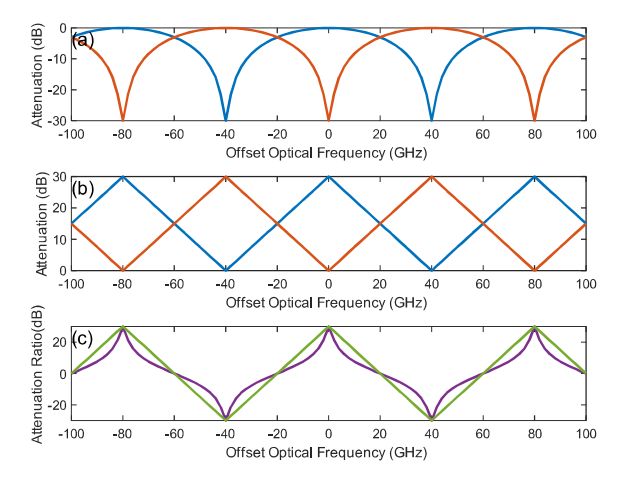


Fig. 2. Simulated transmission curve comparison. (a) sinusoidal transmission curve (log scale); (b) triangular transmission curve (log scale); (c) attenuation slope comparison between sinusoidal (purple) and triangular (green) transmission function.

first-order sidebands are being considered in the model. However, high-order sidebands in non-ideal modulation, varying microwave signal power, as well as frequency (in-)dependent optical/RF noise will significantly affect the frequency estimation model in practical. Since the power ratio between the complementary-filtered output is proportional to the summation of the Bessel functions and the two complementary spectral responses, they can be written as:

$$\begin{split} P_{pos} - P_{inv} &\propto 10 \log_{10} \Sigma_{n} J_{n}^{2}(\beta) \\ &+ 10 \log_{10} \frac{T_{pos}}{T_{inv}} + N(\mu, \sigma_{noise}^{2}) \end{split} \tag{2}$$

where P_{pos} and P_{inv} are the optical power in log scale experiencing positive and inverse transmission responses, respectively. T_{pos} and T_{inv} are the transmission functions of the complementary output of the comb filter. $N(\mu, \sigma_{noise}^2)$ is the unknown instantaneous noise following a Gaussian distribution with mean μ and variance σ_{noise}^2 in the case of central limit theorem [9], which include shot noise, relative intensity noise, and thermal noise.

B. Improved Transfer Function

Conventionally, complementary comb-like spectral response can be obtained easily by putting birefringence medium in an interferometric structure, such that a sinusoidal transfer function can be obtained, as depicted in Fig. 2(a) [10],

$$T(dB) = 10\log_{10}\left[1 - \gamma\cos\left(\frac{f_{RF}}{FSR}\right)\right]$$
 (3)

where γ , f_{RF} , and FSR define the peak-notch contrast ratio, microwave frequency, and free spectral range of the comb filter pair, respectively. However, the resultant spectral response drifts easily with small environmental variations, and the spectral response is sensitive to the polarization of the incident light. Furthermore, the inherent sinusoidal transfer function results in nonlinear mapping between the optical attenuation ratio and the signal frequency, causing a large error variation especially in the peak and notch regions. To control the complementary spectral responses with large degree of freedom and high stability, a programmable wave shaper [11] is utilized in this work instead. Furthermore, a linear triangular transmission function T (depicted in Fig. 2(b)) is used instead of a sinusoidal function to increase the linear range,

$$T(dB) = \max\left(ER - \frac{ER}{FSR/2}|f_{RF}|, 0\right)$$
 (4)

where *ER* is the peak-notch extinction ratio of the complementary triangular spectral responses. Figure 2(c) shows the simulated attenuation ratio comparison between a sinusoidal spectral response and a triangular spectral response. It is observed that the attenuation ratio resulted from the triangular spectral function (green) is highly linear over the whole frequency range of interest, while the attenuation ratio resulted conventional sinusoidal spectral function (purple) is merely linear within a narrow spectral range in the middle of the slope. The nonlinear region introduces inconsistent variations in the relationship between the attenuation ratio and frequency relationship over different frequency, resulting in large measurement error variance. To compare the performance

between a triangular and sinusoidal spectral function for frequency estimation, we define a new parameter, attenuation ratio slope, which describe both the linearity of the spectral function and measurement resolution. In principle, a constant slope across the frequency range of interest is desired to mitigate the errors resulted from nonlinearity in the spectral function. Figure 3 shows the attenuation ratio slope at different FSR and frequency offset from the carrier frequency. The attenuation ratio slope of the triangular spectral function has a constant value over frequency (Fig. 3(c)) while the sinusoidal spectral function has inconsistent attenuation ratio slope. (Fig.3) (a)). Furthermore, for a given FSR, the attenuation ratio slope is consistent for a large range of extinction ratio (ER) in the triangular spectral response (Fig. 3(d)) but varies a lot in the sinusoidal spectral response (Fig.3 (b)). Thus, it is inevitable that frequency estimation error is high at low and high frequency ranges than the center frequency ranges in the sinusoidal case, resulting in a frequency estimation model with large mean squared error.

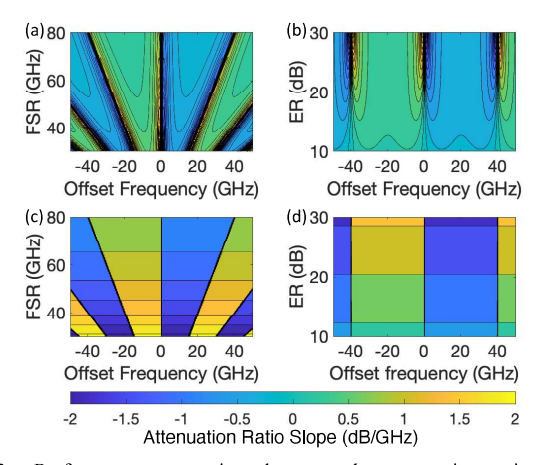


Fig. 3. Performance comparison between the attenuation ratio slope in sinusoidal and triangular spectral response. (a) sinusoidal with fixed ER; (b) sinusoidal with fixed FSR; (c) triangular with fixed ER; (d) triangular with fixed FSR.

C. Data-Driven Model Using Neural Network

Fig. 4 (b) shows the block diagram that describes the workflow of the proposed data-driven frequency estimation scheme: First, the collected data are loaded from the database. Then, data preprocessing is applied, which consists of labeling data, cleaning the data by removing the useless data points, and normalize the data. Next, data partitioning is used to split the data into training data and test data. It is worth to notice that 10-fold cross validation is used, such that 10 different randomly divided data partitions are resulted. Lastly, model inference is performed with testing data, and the metrics are calculated once the model is trained using training data.

DNN is uniquely designed to assist the frequency estimation process in our experiment, that utilize information including measured RF frequency, FSR and ER of the complementary spectral functions, input RF power, and measured optical powers after the complementary spectral filter pair. To train the DNN, the collected data are partitioned into three parts, 90% for training, 5% for validation, and 5% for testing. The designed deep neural network is optimized by adjusting the weights and

bias with Levenberg Marquardt regularization. Specifically, the updated weight and bias parameters during each iteration is equal to $-[J^TJ + \mu I]^{-1}J^Te$, where I is the identity matrix, J is the Jacobian matrix that contains the first derivatives of network errors with respect to the weights and biases, and e is the vector of network errors. Before training, the raw data is normalized into a more understandable format that has a standard deviation of 1 with a mean of 0. The proposed data-driven DNN is then trained in a processer with an Intel Xeon CPU E5 3.5 GHz and two NVIDIA Geforce-Quadro-P4000 GPUs. The trained dataset consists of 14896 observations, which is applied to the designed three-hidden layer DNN, where each layer consists of 10, 20, and 5 neurons, respectively.

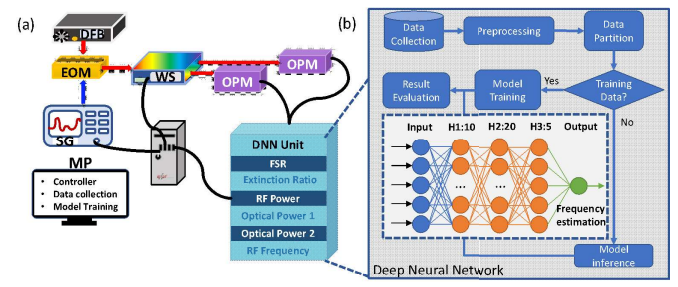


Fig. 4. The proposed data-driven photonic microwave frequency estimation system with improved resolution and immunity to system nonlinearity. (a) Experimental setup. DFB: distributed feedback laser; EOM: electro-optic modulator; SG: signal generator; WS: optical wave shaper; OPM: optical power meter; MP: microprocessor; DNN: deep neural network; (b) structure of the designed DNN, and the overall block diagram showing the workflow of the proposed data-driven evaluation methods.

III. EXPERIMENTAL SETUP

Figure 4(a) shows the experimental setup of the proposed data-driven frequency estimation system that consists of two parts: a complementary optical power measurement unit and a deep neural network for frequency estimation. To achieve complementary optical power measurement, a distributed feedback laser (DFB) centered at 1549.275 nm is used as the optical carrier. To collect training data, an RF signal of interest that sweeps from 1 to 16 GHz with a step of 200 MHz is used. The RF signal is then modulated onto the optical carrier using a 10-Gb/s electro-optic intensity modulator (EOM). The EOM is biased at the null transmission point to achieve CS-DSB modulation, as shown by the blue curve in Fig. 5(a). The CS-DSB optical signal is then passed through the pair of triangular complementary spectral responses (orange curve in log scale) at the optical wave shaper. Triangular response is used to ensure the power difference between the two measured complementary power is proportional to the signal frequency. Transmission outside of the triangular cycle is set to zero for removing optical noise and undesired high frequency harmonics generated during electro-optic modulation. Fig. 5(a) shows the triangular spectral response with variable FSR and ER. In our experiment, FSR ranges from 40 GHz to 70 GHz with step resolution of 5 GHz is used. A larger FSR supports a wider frequency estimation range but would results in a lower frequency resolution. Frequency resolution can be improved by increasing the ER of the triangular spectral response. ER ranges can be set from 15 dB to 30 dB with 5 dB step size. To enable signal power

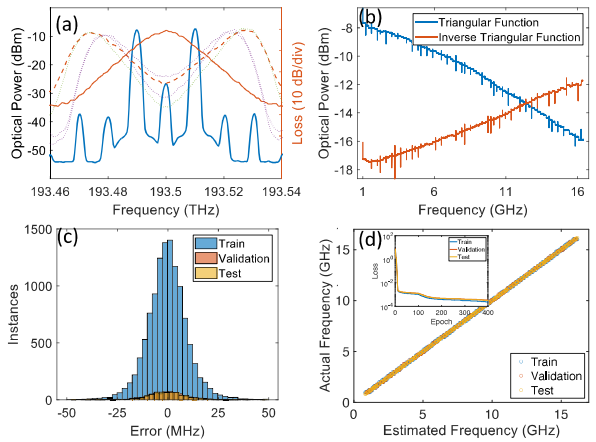


Fig. 5. Examples of various measurement using one setting: (a) Measured optical spectra of CS-DSB signal (blue); complementary triangular transmission curves (orange solid and dash), transmission curves with tunable FSR and ER (purple dotted curves); (b) measured optical power at different RF frequency (RF power = 0 dBm, ER = 15dB and FSR = 0.05THz); (c) Model error distribution among train, validation, and test data; (d) model evaluation with R2 equal to 0.9994 (inset: training, validation and testing loss curves). transparent frequency estimation, training data with RF power from -10 dBm to 2 dBm and increment of 2 dB is used to train the DNN model. A quasi-linear relationship is observed in the measured complementary optical powers obtained through the two triangular complementary spectral responses, as shown in Fig. 5(b).

IV. RESULTS AND DISCUSSION

To evaluate the performance of the trained model, histogram of the absolute error between the predicted and actual RF frequency is shown by the yellow bars in Fig. 5(c), which is less than 50 MHz. The histogram of the training and validation processes are also shown in blue and orange in Fig. 5(c) for comparison. In addition, the calculated RMSE is 1.1 MHz, which correspond to only 0.5% of the RF frequency sweeping step resolution. The regression performance plot between predicted and the actual RF frequency with respect to the training, testing and validation dataset is shown in Fig. 5(d). The calculated R2 value is 99.94% among all groups of data, indicating a goodness of fit of the proposed DNN model. The

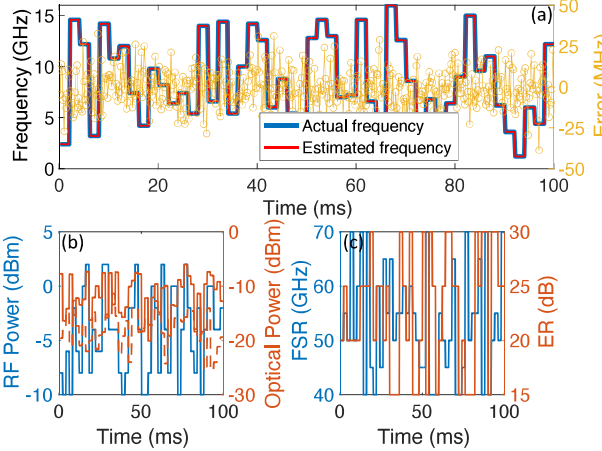


Fig. 6. Performance evaluation: Estimated frequency and true frequency at different system settings. (a) the estimated frequency and true frequency; (b) preset RF power and measured optical power at complementary triangular spectral functions; (c) preset FSRs and ERs.

DNN-assisted frequency estimation system works well even under dynamic user-defined settings with unknown frequency.

To evalute the perfomance of the trained DNN, we apply the new input data to obtain the estimated frequency and compare the result with the actual frequency. In Fig. 6(a), the thick blue line represents the estimated frequency, which matches well with the actual frequency (thin red line). The corresponding RF powers, FSRs, ERs, and measured optical powers are also shown in Fig. 6(b)-(c). The results has a measurement error of less than 50 MHz, proving the successful implementation of DNN-assisted microwave frequency estimation.

V. CONCLUSION

We proposed and experimentally demonstrated a data-driven instantaneous frequency estimation system based on complementary optical power measurement. The absolute measurement error is significantly reduced to 50 MHz with a RMSE of only 1.1 MHz. Compared with the methods without transmission curve improvement and machine learning, the designed DNN-assisted frequency estimation system could solve the precision issues resulted from system noise and device nonlinearity, as well as overfitting problem in most conventional frequency estimation methods. Unlike conventional frequency estimation scheme, the proposed frequency estimation model works well for both pre-known and un-known data. With DNN training, the measurement error is significantly improved through the training and validation process, which also results in high adaptability to unknown RF signal properties.

REFERENCES

- [1] P. Ghelfi, F. Scotti, D. Onori, and A. Bogoni, "Photonics for ultrawideband RF spectral analysis in electronic warfare applications," *IEEE Journal of Selected Topics in Quantum Electronics*, vol. 25, no. 4, pp. 1-9, 2019.
- [2] T. A. Nguyen, E. H. Chan, and R. A. Minasian, "Instantaneous high-resolution multiple-frequency measurement system based on frequency-to-time mapping technique," *Optics letters*, vol. 39, no. 8, pp. 2419-2422, 2014
- [3] J. Niu et al., "Instantaneous microwave frequency measurement based on amplified fiber-optic recirculating delay loop and broadband incoherent light source," *Journal of lightwave technology*, vol. 29, no. 1, pp. 78-84, 2010
- [4] F. Xin, J. Yan, and Q. Liu, "Microwave frequency measurement based on optical phase modulation and stimulated Brillouin scattering," *Electronics Letters*, vol. 53, no. 14, pp. 937-939, 2017.
- [5] M. P. Fok, "Compact and low-latency instantaneous frequency measurement using 38 cm bismuth-oxide fiber and fiber Bragg gratings," *Applied optics*, vol. 52, no. 23, pp. 5659-5662, 2013.
- [6] F. N. Khan, Q. Fan, C. Lu, and A. P. T. Lau, "An optical communication's perspective on machine learning and its applications," *Journal of Lightwave Technology*, vol. 37, no. 2, pp. 493-516, 2019.
- [7] X. Zou, S. Xu, S. Li, J. Chen, and W. Zou, "Optimization of the Brillouin instantaneous frequency measurement using convolutional neural networks," *Optics letters*, vol. 44, no. 23, pp. 5723-5726, 2019.
- [8] Q. Liu and M. P. Fok, "Data-Driven Complementary Power Measurement for Microwave Instantaneous Frequency Estimation," 2021 IEEE Research and Applications of Photonics in Defense Conference (RAPID), 2021, pp. 1-2.
- [9] A. Yariv, P. Yeh, and A. Yariv, *Photonics: optical electronics in modern communications*. Oxford University Press New York, 2007.
- [10] Q. Liu and M. P. Fok, "Dual-Function Frequency and Doppler Shift Measurement System using a Phase Modulator Incorporated Lyot Filter," in 2019 Optical Fiber Communications Conference and Exhibition (OFC), 2019: IEEE, pp. 1-3.
- [11] Q. Liu and M. P. Fok. "Adaptive photonic RF spectral shaper." Optics Express vol. 28, no. 17, pp. 24789-24798, 2020.